Polarized spectroscopy and diode-pumped laser operation of disordered Yb:Ca_3Gd_2(BO_3)_4crystal

Zhongben Pan, Zhang-Lang Lin, Pavel Loiko, Ge Zhang, Huang-Jun Zeng, Wen-Ze Xue, Patrice Camy, Valentin Petrov, Sami Slimi, Xavier Mateos, et al.

▶ **To cite this version:**

Zhongben Pan, Zhang-Lang Lin, Pavel Loiko, Ge Zhang, Huang-Jun Zeng, et al.. Polarized spectroscopy and diode-pumped laser operation of disordered Yb:Ca_3Gd_2(BO_3)_4crystal. Optical Materials Express, 2022, 12 (2), pp.673. 10.1364/OME.449829 . hal-03858693

HAL Id: hal-03858693
https://hal.science/hal-03858693

Submitted on 18 Nov 2022

HAL is a multi-disciplinary open access archive for the deposit and dissemination of scientific research documents, whether they are published or not. The documents may come from teaching and research institutions in France or abroad, or from public or private research centers.

L'archive ouverte pluridisciplinaire **HAL**, est destinée au dépôt et à la diffusion de documents scientifiques de niveau recherche, publiés ou non, émanant des établissements d'enseignement et de recherche français ou étrangers, des laboratoires publics ou privés.

Research Article | Vol. 12, No. 2 / 1 Feb 2022 / Optical Materials Express 673
Optical Materials EXPRESS

Polarized spectroscopy and diode-pumped laser operation of disordered Yb:$Ca_3Gd_2(BO_3)_4$ crystal

Zhongben Pan,[1,2] Zhang-Lang Lin,[2] Pavel Loiko,[3] Ge Zhang,[2] Huang-Jun Zeng,[2] Wen-Ze Xue,[2] Patrice Camy,[3] Valentin Petrov,[4] Sami Slimi,[5] Xavier Mateos,[5] Francesc Díaz,[5] Haifeng Lin,[6] Li Wang,[4] and Weidong Chen[2,4,*]

[1]Institute of Chemical Materials, China Academy of Engineering Physics, 621900 Mianyang, China
[2]Fujian Institute of Research on the Structure of Matter, Chinese Academy of Sciences, 350002 Fuzhou, China
[3]Centre de Recherche sur les Ions, les Matériaux et la Photonique (CIMAP), UMR 6252 CEA-CNRS-ENSICAEN, Université de Caen Normandie, 6 Boulevard Maréchal Juin, 14050 Caen Cedex 4, France
[4]Max Born Institute for Nonlinear Optics and Short Pulse Spectroscopy, Max-Born-Str. 2a, 12489 Berlin, Germany
[5]Universitat Rovira i Virgili (URV), Física i Cristal·lografia de Materials i Nanomaterials (FiCMA-FiCNA), Marcel.li Domingo 1, 43007 Tarragona, Spain
[6]College of Physics and Optoelectronic Engineering, Shenzhen University, Shenzhen 518118 Guangdong, China
*chenweidong@fjirsm.ac.cn

Abstract: We report on the growth, structure, polarized spectroscopy and efficient continuous-wave laser operation of an Yb^{3+}-doped disordered calcium gadolinium borate crystal, Yb^{3+}:$Ca_3Gd_2(BO_3)_4$ (Yb:GdCB). Yb:GdCB belongs to the orthorhombic class [sp. gr. *Pnma*, lattice parameters $a = 7.1937(0)$ Å, $b = 15.5311(3)$ Å, $c = 8.6140(7)$ Å]. The structure disorder of this material originates from a random distribution of Ca^{2+} and $Gd^{3+}|Yb^{3+}$ cations over three non-equivalent lattice sites. This leads to broad and smooth ("glassy-like") absorption and emission spectra at room and low temperatures. The stimulated-emission cross-section of Yb^{3+}, σ_{SE} is 0.42×10^{-20} cm^2 at 1025.1 nm for light polarization $\boldsymbol{E} \parallel \boldsymbol{c}$ and the luminescence lifetime of the $^2F_{5/2}$ state is 644 μs. Continuous-wave laser performance of the Yb:GdCB crystal was evaluated under high-power diode-pumping at 976 nm for three crystal orientations along the crystallographic axes. For an $\boldsymbol{a}$-cut crystal, a maximum output power of 5.58 W was achieved at ~1057 nm with a slope efficiency of 51.7% and a linear laser polarization ($\boldsymbol{E} \parallel \boldsymbol{c}$). The demonstrated power scaling capabilities and broadband emission properties of Yb:GdCB indicate that it is promising for generation of sub-50 fs pulses from passively mode-locked lasers at ~1 μm.

© 2022 Optica Publishing Group under the terms of the Optica Open Access Publishing Agreement

1. Introduction

Borates represent an important class of host crystals very suitable for doping with ytterbium (Yb^{3+}) ions for highly efficient laser operation at ~1 μm. The monoclinic (sp. gr. C*m*) calcium rare-earth oxoborates, $Ca_4REO(BO_3)_3$, where RE = Y and Gd (abbreviated YCOB and GdCOB, respectively) [1,2] represent just one such example. They feature good thermal and thermo-optical properties [3–5], high doping levels (tens of at.%) and attractive spectroscopic properties for Yb^{3+} doping [6], such as large ground-state splitting ($^2F_{7/2}$, >1000 cm^{-1}) leading to broad wavelength

#449829 https://doi.org/10.1364/OME.449829
Journal © 2022 Received 1 Dec 2021; accepted 12 Jan 2022; published 24 Jan 2022

Optical Materials EXPRESS

tuning and low lasing threshold, strongly polarized and broad emission spectra, a relatively long fluorescence lifetime ($^2F_{5/2}$, >2.6 ms), and high absorption cross-sections at zero-phonon line (ZPL) suitable for in-band pumping by commercial high power InGaAs diode lasers at ~980 nm. Efficient and high-power continuous-wave (CW) [4,7] diode-pumped lasers (including thin-disk one [8]) based on such crystals were demonstrated. Due to their disordered structure, Yb^{3+}-doped YCOB and GdCOB crystals exhibit relatively broad and flat gain profiles supporting sub-100 fs pulse generation from mode-locked (ML) lasers [9,10].

There exists another type of Yb^{3+}-doped disordered borate crystals, i.e., Yb^{3+}-doped calcium borate crystal, i.e., Yb:$Ca_3RE_2(BO_3)_4$, where RE stands for Y, Gd or La. They are orthorhombic (sp. gr. *Pnma*). In the host crystals, the cations (M: Ca^{2+} and RE^{3+}) statistically occupy three non-equivalent crystallographic sites (M1, M2 and M3). The crystal structure is composed of three sets of M-oxygen distorted polyhedrons (MO_n) and three sets of isolated BO_3 planar triangles [11,12]. The dopant ions (Yb^{3+}) replace for the RE^{3+} cations in all three M1 – M3 sites. This leads to a variety of multi-ligands around the active ions and a pronounced inhomogeneous spectral line broadening. Thus, the absorption and luminescence spectra of Yb^{3+} ions in $Ca_3RE_2(BO_3)_4$ crystals resemble those in borate glasses (a "glassy-like" spectroscopic behavior). This makes Yb:$Ca_3RE_2(BO_3)_4$ crystals attractive for ML lasers.

Calcium gadolinium borate, $Ca_3Gd_2(BO_3)_4$ (abbreviated: GdCB), represents one of these disordered materials displaying extraordinary spectroscopic features when doped with Yb^{3+} ions. By virtue of the Ca^{2+} and $Gd^{3+}|Yb^{3+}$ cations statistically occupying the M1 – M3 lattice sites [13], Yb:GdCB manifests a "glassy-like" spectroscopic behavior at the cost of a relatively low thermal conductivity of 0.92 W/mK at room temperature [14]. It melts congruently at a relatively low temperature of 1400°C and it can be easily grown by the conventional Czochralski (Cz) method [15]. So far, only unpolarized spectroscopic properties of the Yb:GdCB crystal were investigated at room temperature (RT) [13]. Xu *et al.* reported on a CW Yb:GdCB laser pumped by a multi-transverse mode fiber-coupled InGaAs diode laser at 976 nm yielding an output power of 1.4 W at ~1060 nm with a relatively low slope efficiency of 23.7% [16]. Zeng *et al.* demonstrated a diode-pumped Yb:GdCB laser ML by a semiconductor saturable absorber mirror delivering pulses as short as 96 fs at 1045 nm with an average output power of 205 mW at a pulse repetition rate of 67.3 MHz [17].

In the present work, we report on the crystal growth, structure refinement, polarized RT, as well as low temperature (LT, 10 K) spectroscopy, and efficient and power-scalable CW laser operation of the Yb:GdCB crystal at ~1 μm. Our results indicate the prospects of the Yb:GdCB crystal for ultrashort pulse generation, as well as for power scalable operation.

2. Crystal growth and structure

2.1. Crystal growth

A 5 at.% Yb^{3+} (in the melt) doped GdCB crystal was grown by the Cz method under an argon (Ar) atmosphere in an iridium crucible. The starting materials were $CaCO_3$ (4N), Gd_2O_3 (5N), H_3BO_3 (5N) and Yb_2O_3 (5N). They were weighed according to the stoichiometric composition with 5 at.% Yb^{3+} (with respect to Gd^{3+}), $Ca_3Gd_{1.9}Yb_{0.1}(BO_3)_4$, and an excess of 3 wt% H_3BO_3 was added to compensate the evaporation of B_2O_3 during the crystal growth. The compound was synthesized via the following solid-state reaction:

$$6Ca_2CO_3 + 8H_3BO_3 + 1.9Gd_2O_3 + 0.1Yb_2O_3 \rightarrow 2Ca_3Gd_{1.9}Yb_{0.1}(BO_3)_4 + 12H_2O\uparrow + 6CO_2\uparrow.$$

For that, the starting materials were mixed, ground and heated at 1173 K for 10 hours (h) in a platinum crucible. Once the crucible cooled down to RT, the mixture was pressed into pellets and reheated at 1373 K for 10 h. The synthesized polycrystalline material was placed in an iridium crucible and melted by an intermediate-frequency heater. To release the bubbles in the melt and

Optical Materials EXPRESS

to avoid the formation of polycrystals during the crystal growth process, a temperature of 30 - 50 K higher than the melting point is required. The melt was held at this temperature for about 2 - 3 h before starting the growth. An [010] oriented seed from undoped GdCB was used. After dipping the seed into the melt and adjusting the heating power of the furnace, the crystal growth was performed with a pulling rate of 0.5 - 2.0 mm/h and a rotation speed of 10 - 15 revolutions per minute. After growth was completed, the crystal was slowly removed from the melt and cooled down to RT at a stepped rate of 15 to 25 K/h.

Figure 1 shows a photograph of an as-grown Yb:GdCB crystal boule. It had a cylindrical shape with dimensions of $\Phi\ 20 \times 25\ mm^2$. The crystal did not display any cracks, inclusions and scattering centers under illumination by a He-Ne laser, indicating an excellent optical quality. It was colorless and transparent.

Fig. 1. Photograph of an as-grown 5 at.% Yb:GdCB crystal.

The actual doping level was determined by Inductively Coupled Plasma Mass Spectrometry (ICP-MS) to be $N_{Yb} = 4.15 \times 10^{20}/cm^3$ (5.0 at.%). The segregation coefficient for Yb^{3+} ions, $K_{Yb} = C_{crystal}/C_{melt}$, was close to unity.

2.2. Structure refinement

The crystal structure and the phase purity were confirmed by X-ray powder diffraction (XRD). The XRD pattern was measured using a Bruker D2 Phaser diffractometer with CuKα radiation (1.5418 Å) in the range of diffraction angles $2\theta = 10–88°$ with a step size of 0.02° and a step time of 2 s. All the reflections in the XRD pattern were assigned to a single crystalline phase isostructural to undoped GdCB.

The crystal structure of 5 at.% Yb:GdCB was refined by the Rietveld method using the Match3 software. The structural data for $Ca_3Y_2(BO_3)_4$ [12] were taken as a starting model. The observed, calculated and residual XRD patterns are shown in Fig. 2. Yb:GdCB belongs to the orthorhombic class (sp. gr. $Pnma - D_{2h}^{16}$, No. 62) with lattice constants $a = 7.1937(0)$ Å, $b = 15.5311(3)$ Å, $c = 8.6140(7)$ Å (number of formula units per unit-cell: $Z = 4$). The unit-cell volume is $V = 962.419$ Å^3 and the calculated crystal density $\rho_{calc} = 4.790\ g/cm^3$. The refinement R-factors are $R_{wp} = 2.97\%$, $R_{exp} = 1.67\%$ and $\chi^2 = (R_{wp}/R_{exp})^2 = 3.16$ indicating good convergence of the fit. More details about the Rietveld refinement can be found in Table 1. The refined lattice parameters of Yb:GdCB are slightly smaller compared to undoped GdCB [$a = 7.1953(3)$ Å, $b = 15.5348(7)$ Å and $c = 8.6197(4)$ Å] [14], due to the difference in ionic radii of Yb^{3+} (0.985 Å) and Gd^{3+} (1.053 Å) for VIII-fold oxygen coordination.

Table 2 shows the fractional atomic coordinates (x, y, z), the site occupancy factors (O.F.) and the isotropic displacement parameters B_{iso} obtained via the Rietveld refinement. There exist three non-equivalent cationic sites: M1 – 4c, M2 – 8d and M3 – 8d (designation – Wyckoff symbol). They are statistically occupied by Ca^{2+}, Gd^{3+} and Yb^{3+}. The corresponding O.F. are: 0.390 - 0.575 - 0.035 (M1), 0.555 - 0.425 - 0.020 (M2) and 0.750 - 0.235 - 0.015 (M3).

Optical Materials EXPRESS

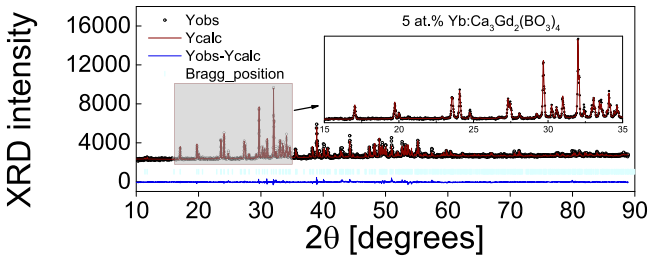

Fig. 2. Rietveld refinement plots for the 5 at.% Yb:GdCB crystal: the experimental (Y_{obs}), the calculated (Y_{calc}) and the difference (Y_{obs} - Y_{calc}) patterns, *vertical dashes* - the Bragg positions; *Inset*: zoomed view on the 2θ range of 15 - 35°.

Table 1. Rietveld Refinement Data for the 5 at.% Yb:GdCB

Parameter	Value
Crystal system	Orthorhombic
Space group (IT number)	*Pnma* – D_{2h}^{16} (No. 62)
Number of formula units	$Z = 4$
Reduced number of S.O.	4
General multiplicity	8
Calculated density (g/cm^3)	4.790
Lattice constant *a*, *b*, *c* (Å)	7.1937(0), 15.5311(3), 8.6140(7)
Unit-cell volume *V* (Å^3)	962.419
2θ range (deg)	10–88
2θ step (deg)	0.02
Radiation	Cu-Kα1 ($\lambda = 1.5418$ Å)
No. of reflections	862
Refinement software	Match3 (crystal impact) software
Reliability factors	$R_p = 2.09\%$, $R_{wp} = 2.97\%$, $R_{exp} = 1.67\%$ and $\chi^2 = 3.16$

Table 2. Fractional Atomic Coordinates (x, y, z), Sites, Occupancy Factors (O.F.) and Isotropic Displacement Parameters B_{iso} for 5 at.% Yb:GdCB

Atom	Wyckoff	*x*	*y*	*z*	O.F.	B_{iso}, Å^2
M1[a]s	4*c*	0.1740(0)	1/4	0.9651(0)	0.390 - 0.575 - 0.035	1.959(0)
M2	8*d*	-0.0199(1)	0.4164(1)	0.6759(6)	0.555 - 0.425 - 0.020	1.269(0)
M3	8*d*	-0.1969(5)	0.3729(5)	1.1566(0)	0.750 - 0.235 - 0.015	0.552(0)
B1	4*c*	0.4925(7)	1/4	1.1030(0)	1	1.421(0)
B2	4*c*	0.3031(0)	1/4	0.6293(6)	1	1.026(0)
B3	8*d*	0.2988(9)	0.5357(9)	0.5058(3)	1	1.658(0)
O1	8*d*	0.4641(0)	0.33068	1.0708(0)	1	3.158(0)
O2	4*c*	0.1502(5)	1/4	1.2367(0)	1	3.158(0)
O3	4*c*	-0.1867(4)	1/4	1.0079(0)	1	3.158(0)
O4	8*d*	0.2037(5)	0.4910(0)	0.4884(1)	1	3.158(0)
O5	8*d*	-0.1103(0)	0.5336(4)	0.8169(5)	1	3.158(0)
O6	8*d*	-0.2430(2)	0.3147(7)	0.7670(2)	1	3.158(0)
O7	8*d*	0.1095(4)	0.3878(5)	0.9494(5)	1	3.158(0)

[a]M = Ca, Gd and Yb.

Optical Materials EXPRESS

A fragment of the crystal structure is shown in Fig. 3(a), drawn according to the refined structural data using the Diamond4 program. The structure of Yb:GdCB is determined by facet- and edge-sharing M-oxygen (MO_n) polyhedra of an irregular shape separated by isolated BO_3 triangles. The species in M1 sites are surrounded by eight oxygen atoms with bond distances ranging from 2.1947(6) to 2.6211(1) Å, while the species in M2 and M3 sites are coordinated by seven oxygen atoms with bond distances ranging from 2.2839(9) Å to 2.5884(8) Å and from 2.3005 (5) to 2.6994 (9) Å, respectively. Each M3-based polyhedron is surrounded by four M1- and four M2-based polyhedra, Fig. 3, creating a disordered pseudo-cube with the M3 polyhedron inside and the M1- or M2-based polyhedra at the corners. The M1- and M2-based polyhedra from two neighboring pseudo-cubes are lying approximately within the same ***a*-*b*** plane. The full set of interatomic distances for M-oxygen polyhedra is given in Table 3.

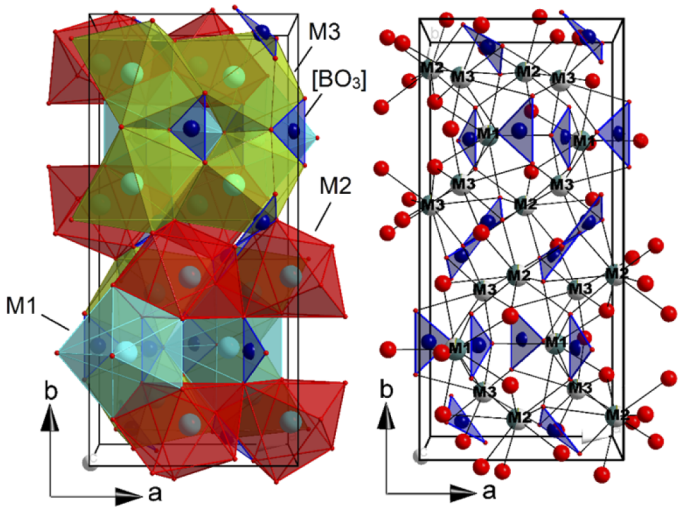

Fig. 3. A fragment of the crystal structure of 5 at.% Yb:GdCB: (a) a projection onto the ***a*-*b*** plane showing the different M-oxygen polyhedra; (b) local environment around the cationic sites M1, M2 and M3.

Table 3. Selected Interatomic Distances for 5 at.% Yb:GdCB

M1 – O, Å		M2 - O, Å		M3 - O, Å	
M1-O3 = 2.6211(1)	1	M2-O1 = 2.5107(5)	1	M3-O5 = 2.6532(2)	1
M1-O7 = 2.1947(6)	2	M2-O6 = 2.3838(4)	1	M3-O1 = 2.6994(9)	1
M1-O2 = 2.3458(1)	1	M2-O4 = 2.4129(5)	1	M3-O3 = 2.3005(5)	1
M1-O6 = 2.3165(2)	1	M2-O5 = 2.2839(9)	1	M3-O2 = 2.3873(4)	1
M1-O1 = 2.5989(0)	2	M2-O4 = 2.5575(2)	1	M3-O5 = 2.4358(7)	1
M1-O6 = 2.3165(2)	1	M2-O7 = 2.5715(9)	1	M3-O4 = 2.3307(4)	1
		M2-O6 = 2.5884(8)	1	M3-O1 = 2.6310(8)	1

3. Optical spectroscopy

The RT transmission spectrum of a 1 mm-thick 5 at.% Yb:GdCB crystal is shown in Fig. 4. In the visible, no signs of absorption due to color centers and Yb^{2+} ions are observed. The absorption at ~1 μm is due to the $^2F_{7/2} \rightarrow {}^2F_{5/2}$ transition of the Yb^{3+} ion. In the UV, the sharp bands at

Optical Materials EXPRESS

274 - 280 nm and 301–312 nm are due to the host-forming Gd^{3+} ion. The UV absorption edge of the host matrix is observed at ~255 nm.

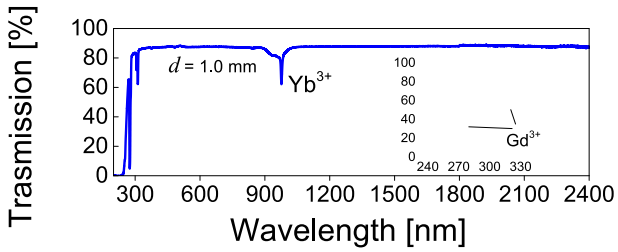

Fig. 4. RT unpolarized transmission spectrum of a 1 mm-thick 5 at.% Yb:GdCB crystal plate, *inset* – a close look at the UV spectral range.

Orthorhombic Yb:GdCB is an optically biaxial crystal. Thus, its spectral properties were characterized for three principal light polarizations, $\boldsymbol{E} \parallel \boldsymbol{a}$, $\boldsymbol{b}$ and $\boldsymbol{c}$. The polarized RT absorption (σ_{abs}) cross-section spectra of Yb:GdCB are shown in Fig. 5. The maximum σ_{abs} reaches 0.99×10^{-20} cm^2 at 976.5 nm (ZPL) and the corresponding absorption bandwidth (determined at full width at half maximum, FWHM) is 7.3 nm for light polarization $\boldsymbol{E} \parallel \boldsymbol{b}$. Such a broad bandwidth releases the limitations for pumping the Yb:GdCB crystals with high-power InGaAs laser diodes related to the possible temperature drift of the diode wavelength. For other polarizations, the peak σ_{abs} is lower, 0.74×10^{-20} cm^2 at 977.1 nm ($\boldsymbol{E} \parallel \boldsymbol{a}$) and 0.73×10^{-20} cm^2 at 976.8 nm ($\boldsymbol{E} \parallel \boldsymbol{c}$), while the absorption bandwidth is similar (7.5 nm).

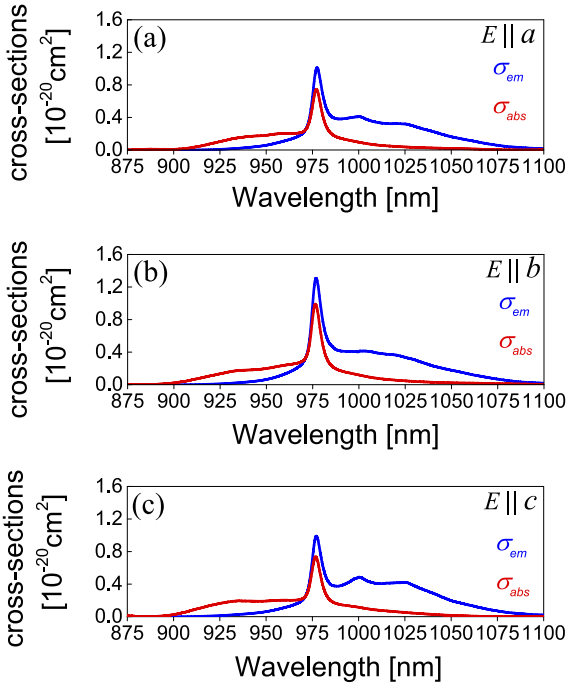

Fig. 5. Polarized RT absorption (σ_{abs}) and stimulated-emission (SE, σ_{SE}) cross-sections of Yb^{3+} in the Yb:GdCB crystal. The light polarization is: (a) $\boldsymbol{E} \parallel \boldsymbol{a}$; (b) $\boldsymbol{E} \parallel \boldsymbol{b}$ and (c) $\boldsymbol{E} \parallel \boldsymbol{c}$.

The stimulated-emission (SE, σ_{SE}) cross-sections were calculated based on a combination of the Füchtbauer–Ladenburg equation and the reciprocity method (RM). A good agreement

Optical Materials EXPRESS

between the two methods (considering the effect of reabsorption on the measured luminescence spectra) was observed for a radiative lifetime of the $^2F_{5/2}$ Yb^{3+} multiplet $\tau_{rad} = 0.65 \pm 0.05$ ms. A mean refractive index $\langle n \rangle = 1.70$ was used for calculations. The combined σ_{SE} spectra are shown in Fig. 5. The maximum σ_{SE} is 1.31×10^{-20} cm^2 at 976.8 nm (ZPL) for light polarization $\boldsymbol{E} \parallel \boldsymbol{b}$. In the spectral range where laser operation is expected (at wavelengths well above the ZPL, >1 μm), σ_{SE} reaches 0.42×10^{-20} cm^2 at 1025.1 nm for $\boldsymbol{E} \parallel \boldsymbol{c}$. For other two polarizations in this spectral range, the peak σ_{SE} is lower, namely 0.36×10^{-20} cm^2 at 1019.9 nm ($\boldsymbol{E} \parallel \boldsymbol{b}$) and 0.32×10^{-20} cm^2 at 1025.0 nm ($\boldsymbol{E} \parallel \boldsymbol{a}$). The intrinsic anisotropy of the SE cross-sections

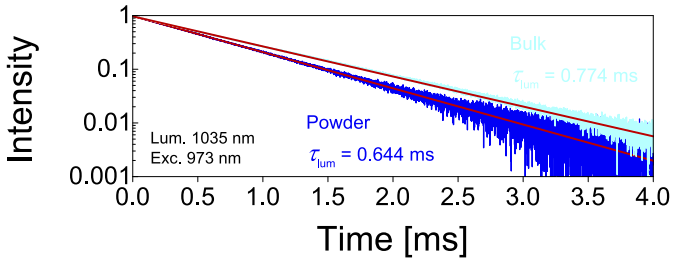

Fig. 6. RT luminescence decay curve for Yb^{3+} ions in the 5 at.% Yb:GdCB crystal (bulk and powdered samples), *red lines* – single-exponential fits, $\lambda_{exc} = 973$ nm, $\lambda_{lum} = 1035$ nm.

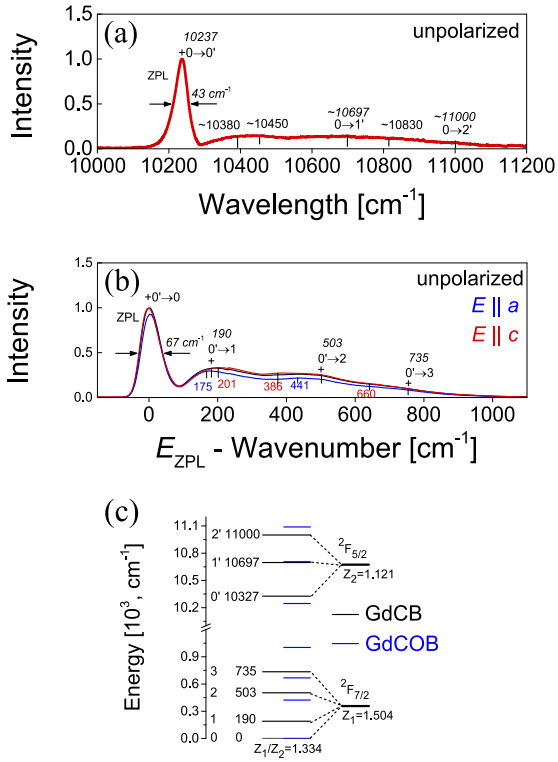

Fig. 7. LT (10 K) spectroscopy of the 5 at.% Yb:GdCB crystal: (a) absorption spectrum and (b) luminescence spectra, $\lambda_{exc} = 973$ nm; (c) suggested energy-level scheme of Yb^{3+} in one of the sites in the GdCB crystal, the data for GdCOB [2] are shown for comparison. $Z_{1(2)}$ are the partition functions.

Optical Materials EXPRESS

indicates that a linearly polarized radiation is expected to be generated from Yb:GdCB lasers without polarization-selective elements (***E*** || ***c*** or ***E*** || ***b***, depending on the crystal cut).

The luminescence decay curve was measured using a finely powdered crystalline sample to avoid the effect of radiation trapping (reabsorption). The Yb^{3+} ion luminescence in GdCB exhibits a single-exponential decay corresponding to a luminescence a lifetime of $\tau_{lum} = 644$ µs, Fig. 6.

It indicates that the transition intensities of Yb^{3+} ions residing in M1 – M3 sites are relatively close. The determined τ_{lum} value agrees well with the estimated radiative lifetime. To further reveal the inhomogeneous spectral broadening for Yb^{3+} ions in GdCB, the LT absorption and luminescence spectra were measured, Fig. 7(a,b). The luminescence was studied under non-selective excitation.

The broadband spectral properties of Yb:GdCB were preserved even at 10 K. The ZPL in absorption centered at 10237 cm^{-1} (976.8 nm) had a bandwidth (FWHM) of 43 cm^{-1} which is at least one order of magnitude broader than that for ordered crystals. An attempt to assign the electronic transitions for one of the Yb^{3+} species in GdCB (the dominant one) was made following the previously reported crystal-field splitting for Yb:GdCOB (site I, Gd) [2]. The energy levels of the ground-state ($^2F_{7/2}$) were numbered as 0–3 and those of the excited-state ($^2F_{5/2}$) – as 0' – 2'. This resulted in the following crystal-field splitting: $^2F_{7/2}$ = (0, 190, 503, 735) cm^{-1} and $^2F_{5/2}$ = (10327, 10697, 11000) cm^{-1}, cf. Figure 7(c). The partition functions for the lower and upper Yb^{3+} manifolds were then calculated to be $Z_1 = 1.504$ and $Z_2 = 1.121$, respectively, yielding a ratio $Z_1/Z_2 = 1.334$ used for the calculations of the SE cross-sections by the reciprocity method.

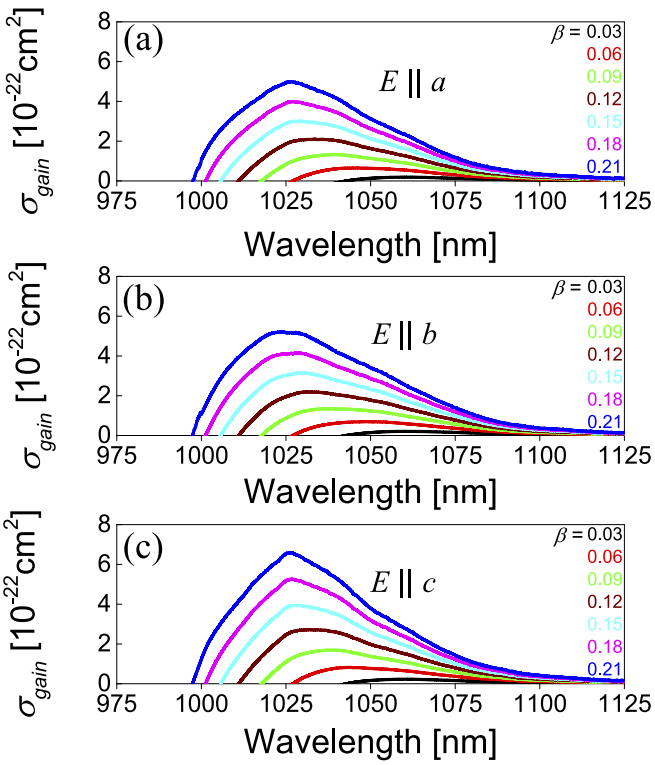

Fig. 8. RT polarized gain cross-section (σ_{gain}) spectra for Yb:GdCB crystal, β is the inversion ratio. The light polarization is: (a) ***E*** || ***a***; (b) ***E*** || ***b*** and (c) ***E*** || ***c***.

Optical Materials EXPRESS

According to the quasi-three-level nature of the Yb laser, the gain cross-sections, $\sigma_{gain} = \beta\sigma_{SE} - (1-\beta)\sigma_{abs}$, were calculated, where $\beta = N_2/N_{Yb}$ is the inversion ratio and N_2 is the population of the upper laser level ($^2F_{5/2}$). The polarized gain profiles are shown in Fig. 8. With increasing the inversion ratio, the spectral maximum shifts to shorter wavelengths, e.g., from 1060 nm for small $\beta = 0.03$ to 1027 nm for high $\beta > 0.15$ (for $\boldsymbol{E} \parallel \boldsymbol{c}$). The gain bandwidths for an intermediate $\beta = 0.12$ are 48 nm ($\boldsymbol{E} \parallel \boldsymbol{a}$), 51 nm ($\boldsymbol{E} \parallel \boldsymbol{b}$) and 46 nm ($\boldsymbol{E} \parallel \boldsymbol{c}$). These values, as well as the extremely broad and smooth gain spectra indicate the high potential of the Yb:GdCB crystal for broadly tunable operation and sub-50 fs pulse generation from ML lasers.

4. Diode-pumped laser operation

The schematic of the diode-pumped compact Yb:GdCB laser is shown in Fig. 9. Three rectangular samples with 5 at.% Yb^{3+} doping were oriented for light propagation along the three crystallographic axes (denoted as ***a***-cut, ***b***-cut and ***c***-cut) having identical dimensions (aperture: 4 mm × 4 mm, thickness: 3 mm). Their input and output faces were polished to laser quality and left uncoated. The crystals were wrapped in Indium foil and repetitively mounted into the same copper holder cooled by circulating water (coolant temperature: 15°C). The pump source was a multi-transverse mode, fiber-coupled InGaAs diode laser emitting up to 50 W of unpolarized radiation at 976 nm. The fiber had a core diameter of 105 μm and a numerical aperture (N.A.) of 0.15. The emission wavelength of the diode laser was locked by a fiber Bragg grating (FBG) over the entire operation range with a linewidth of ~0.7 nm. The pump beam was reimaged into the laser crystal by a pair of antireflection-coated doublet lenses with identical focal lengths ($f = 50$ mm) yielding a beam waist of ~63 μm (radius).

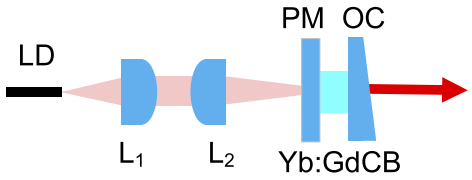

Fig. 9. Schematic of the diode-pumped Yb:GdCB laser. LD: fiber-coupled laser diode; L_1 and L_2: lenses; PM: pump mirror; OC: output coupler.

The laser cavity consisted of a flat pump mirror (PM) coated for high transmission at 0.9-1.01 μm and high reflection at 1.02-1.2 μm, and a plane-wedged output coupler (OC) with a set of transmissions at the laser wavelength ($T_{OC} = 1\%$ - 10%). Both cavity mirrors were placed as close as possible to the laser crystal oriented for normal incidence resulting in a microchip-type design. The geometrical cavity length of such a micro-laser was ~3 mm. The obtained laser operation in a plano-plano cavity with all the studied crystal cuts indicated a positive (focusing) thermal lens in Yb:GdCB for laser polarizations $\boldsymbol{E} \parallel \boldsymbol{b}$ and $\boldsymbol{E} \parallel \boldsymbol{c}$. The maximum incident pump power was limited to 18.7 W to avoid the risk of thermal fracture of the crystal. The single-pass pump absorption efficiency was measured under lasing condition yielding values between 54.4% and 60.1% depending on the crystal orientation and the transmission of the OC.

The CW laser performance for different OCs with the three Yb:GdCB samples of different cuts is shown in Fig. 10. The best performance was observed for the ***a***-cut crystal: the laser generated a maximum output power of 5.58 W at 1045 - 1067 nm (a broad spectrum) with a slope efficiency η of 51.7% (vs. the absorbed pump power) and an optical-to-optical efficiency of 49.7%, Fig. 10(a) (for $T_{OC} = 1\%$). With increasing the output-coupling, the laser threshold gradually increased from 0.137 W ($T_{OC} = 1\%$) to 1.188 W ($T_{OC} = 10\%$). A comparison of these results with those obtained for ***b***-cut and ***c***-cut crystals can be found in Table 4.

Optical Materials EXPRESS

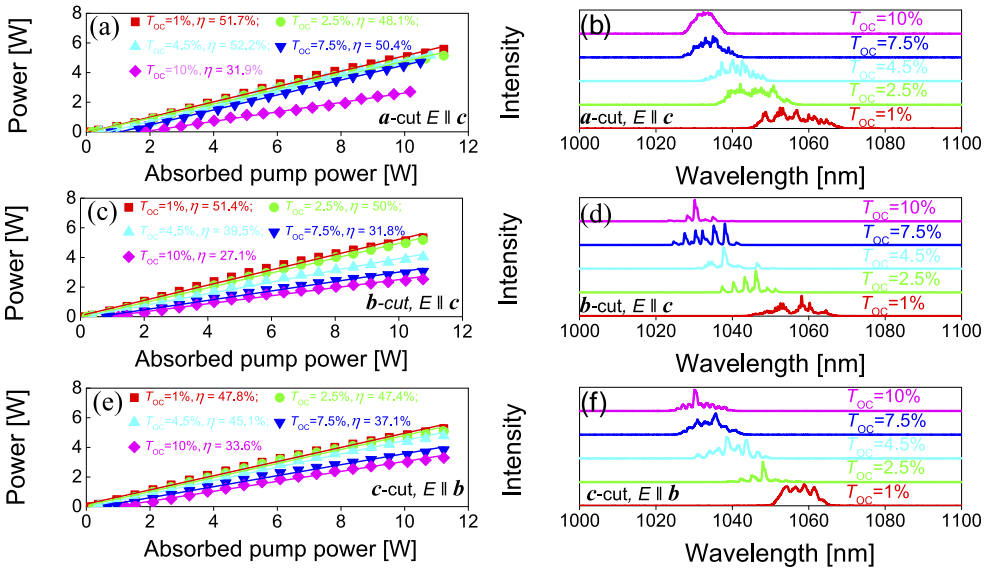

Fig. 10. CW diode-pumped Yb:GdCB lasers: (a), (c) and (e) input – output dependences, η – slope efficiency; (b), (d) and (f) typical spectra of laser emission. Crystal orientation and laser polarization: (a) and (b) ***a***-cut, $\boldsymbol{E} \parallel \boldsymbol{c}$; (c) and (d) ***b***-cut, $\boldsymbol{E} \parallel \boldsymbol{c}$; (e) and (f) ***c***-cut, $\boldsymbol{E} \parallel \boldsymbol{b}$.

Table 4. Continuous-Wave Diode-Pumped Laser Performance[a] of 5 at.% Yb:GdCB Crystals with Different Orientations

Cut	Polarization	P_{out}, W	λ_L, nm	η, %	P_{th}, W	η_{opt}, %
a-cut	$\boldsymbol{E} \parallel \boldsymbol{c}$	5.58	1045–1057	51.7	0.137	49.7
b-cut	$\boldsymbol{E} \parallel \boldsymbol{c}$	5.33	1030–1058	51.4	0.137	49.8
c-cut	$\boldsymbol{E} \parallel \boldsymbol{b}$	5.27	1030–1057	47.8	0.069	46.9

[a] P_{out} – output power, λ_L – laser wavelength, η – slope efficiency, P_{th} – laser threshold, η_{opt} – optical efficiency. T_{OC} = 1%.

For all three crystal cuts, the laser emission was linearly polarized, and the polarization state was naturally selected by the anisotropy of the gain. The laser polarization was $\boldsymbol{E} \parallel \boldsymbol{c}$ (***a***-cut and ***b***-cut crystals) and $\boldsymbol{E} \parallel \boldsymbol{b}$ (***c***-cut crystal). This agrees well with the anisotropy of the SE cross-sections for the Yb^{3+} ions in the GdCB crystal, cf. Figure 5. The same polarization state was preserved over the entire studied range of pump powers. Typical laser emission spectra of the three samples are shown in Fig. 10(b), (d) and (f). They exhibited a similar dependence on the OC transmission, e.g., varying from 1045–1067 nm (T_{OC} = 1%) to 1028–1038 nm (T_{OC} = 10%) for the ***a***-cut crystal. The observation of a red-shift of the laser wavelength with the reduction of the OC transmission is typical for quasi-three-level Yb lasers with intrinsic reabsorption at the laser wavelength and it is in line with the calculated polarized gain cross-section spectra of the Yb:GdCB crystal, cf. Figure 8. The broad free-running spectra are due to the very flat Yb^{3+} gain profiles, and their multi-peak structure is attributed to etalon (Fabry-Perot) effects between the mirror / crystal interfaces.

5. Conclusion

To conclude, Yb^{3+}:$Ca_3Gd_2(BO_3)_4$ (Yb:GdCB), is a promising laser material with broadband emission properties at ~1 μm. It features a variety of cationic sites (M1 – M3) with a distorted VIII-fold (M1) and VII-fold (M2, M3) coordination randomly populated by the Ca^{2+} and

Optical Materials EXPRESS

$Gd^{3+}|Yb^{3+}$ cations leading to an extremely strong inhomogeneous broadening of absorption and emission bands of Yb^{3+} ions (a "glassy-like" spectroscopic behavior). Moreover, it offers a notable polarization-anisotropy of stimulated-emission cross-section spectra which determines a linear polarization in Yb:GdCB lasers (**E** || **b** or **E** || **c**, depending on the crystal orientation). Yb:GdCB is characterized by a large total Stark splitting of the ground-state ($^2F_{7/2}$, 735 cm^{-1}), as well as long fluorescence lifetime (644 μs), which are favorable for low-threshold laser operation. The broad absorption linewidth (~7.3–7.5 nm at 976 nm corresponding to the Yb^{3+} zero-phonon-line (ZPL) releases the constraints on the bandwidth and temperature drift of the emission wavelength for commercially available InGaAs diode lasers. Finally, the extremely broad, flat and smooth gain profiles of the Yb^{3+} ion in GdCB being superior in this regard to those for well-known Yb^{3+}-doped monoclinic calcium oxoborate crystals (e.g., Yb:YCOB and Yb:GdCOB), indicate the high potential of the former crystal for applications in sub-50 fs pulse generation from ML lasers, particularly in terms of shortening the pulse duration of low-to-moderate power seeding lasers for ultrafast amplifiers.

Funding. National Natural Science Foundation of China (61975208, 61875199, 51761135115, 61850410533, 62075090, 52072351); Sino-German Scientist Cooperation and Exchanges Mobility Program (M-0040); National Key Research and Development Program of China (2018YFB2201101); Natural Science Foundation of Fujian Province (2019J02015); Foundation of the President of Foundation of the President of China Academy of Engineering Physics (YZJJLX2018005); Grant PID2019-108543RB-I00 funded by MCIN/AEI; Foundation of Key Laboratory of Optoelectronic Materials Chemistry and Physics, Chinese Academy of Sciences (2008DP173016); Foundation of State Key Laboratory of Crystal Materials, Shandong University (KF2001).

Acknowledgements. This research article has been possible with the support of the Secretaria d'Universitats i Recerca del Departament d'Empresa i Coneixement de la Generalitat de Catalunya, the European Union (UE) and the European Social Fund (ESF) (2020 FI-B 00522); Grant PID2019-108543RB-I00 funded by MCIN/AEI/10.13039/501100011033.

Xavier Mateos is a Serra Húnter Fellow.

Disclosures. The authors declare no conflicts of interest.

Data availability. Data underlying the results presented in this paper are not publicly available at this time but may be obtained from the authors upon reasonable request.

References

1. F. Druon, F. Augé, F. Balembois, P. Georges, A. Brun, A. Aron, F. Mougel, G. Aka, and D. Vivien, "Efficient, tunable, zero-line diode-pumped, continuous-wave Yb^{3+}:$Ca_4LnO(BO_3)_3$ (Ln = Gd, Y) lasers at room temperature and application to miniature lasers," J. Opt. Soc. Am. B **17**(1), 18–22 (2000).
2. F. Mougel, K. Dardenne, G. Aka, A. Kahn-Harari, and D. Vivien, "Ytterbium-doped $Ca_4GdO(BO_3)_3$: An efficient infrared laser and self-frequency doubling crystal," J. Opt. Soc. Am. B **16**(1), 164–172 (1999).
3. P. Loiko, J. M. Serres, X. Mateos, H. Yu, H. Zhang, J. Liu, K. Yumashev, U. Griebner, V. Petrov, M. Aguilo, and F. Diaz, "Thermal lensing and multiwatt microchip laser operation of Yb:YCOB crystals," IEEE Photonics J. **8**(3), 1–12 (2016).
4. P. Loiko, X. Mateos, Y. Wang, Z. Pan, K. Yumashev, H. Zhang, U. Griebner, and V. Petrov, "Thermo-optic dispersion formulas for YCOB and GdCOB laser host crystals," Opt. Mater. Express **5**(5), 1089–1097 (2015).
5. Q. Fang, D. Lu, H. Yu, H. Zhang, and J. Wang, "Anisotropic thermal properties of Yb:YCOB crystal influenced by doping concentrations," Opt. Mater. Express **9**(3), 1501–1512 (2019).
6. A. Aron, G. Aka, B. Viana, A. Kahn-Harari, D. Vivien, F. Druon, F. Balembois, P. Georges, A. Brun, N. Lenain, and M. Jacquet, "Spectroscopic properties and laser performances of Yb:YCOB and potential of the Yb:LaCOB material," Opt. Mater. **16**(1-2), 181–188 (2001).
7. S. Chenais, F. Druon, F. Balembois, G. Lucas-Leclin, P. Georges, A. Brun, M. Zavelani-Rossi, F. Augé, J. P. Chambaret, G. Aka, and D. Vivien, "Multiwatt, tunable, diode-pumped CW Yb:GdCOB laser," Appl. Phys. B **72**(4), 389–393 (2001).
8. C. Kränkel, R. Peters, K. Petermann, P. Loiseau, G. Aka, and G. Huber, "Efficient continuous-wave thin disk laser operation of Yb:$Ca_4YO(BO_3)_3$ in E parallel to Z and E parallel to X orientations with 26 W output power," J. Opt. Soc. Am. B **26**(7), 1310–1314 (2009).
9. A. Yoshida, A. Schmidt, V. Petrov, C. Fiebig, G. Erbert, J. Liu, H. Zhang, J. Wang, and U. Griebner, "Diode-pumped mode-locked Yb:YCOB laser generating 35 fs pulses," Opt. Lett. **36**(22), 4425–4427 (2011).
10. F. Druon, F. Balembois, P. Georges, A. Brun, A. Courjaud, C. Honninger, F. Salin, A. Aron, F. Mougel, G. Aka, and D. Vivien, "Generation of 90-fs pulses from a mode-locked diode-pumped Yb^{3+}:$Ca_4GdO(BO_3)_3$ laser," Opt. Lett. **25**(6), 423–425 (2000).

Optical Materials EXPRESS

11. K. M. Kosyl, W. Paszkowicz, R. Minikayev, A. N. Shekhovtsov, M. B. Kosmyna, M. Chrunik, and A. N. Fitch, "Site-occupancy scheme in disordered $Ca_3RE_{2(}BO_3)_4$: a dependence on rare-earth (RE) ionic radius," Acta Crystallogr B Struct Sci Cryst Eng Mater **77**(3), B77 (2021).
12. Y. Wang, C. Tu, C. Huang, and Z. You, "Study of crystal Yb^{3+}:$Ca_3Y_2(BO_3)_4$," J. Mater. Res. **19**(4), 1203–1207 (2004).
13. C. Tu, Y. Wang, Z. You, J. Li, Z. Zhu, and B. Wu, "Growth and spectroscopic characteristics of $Ca_3Gd_2(BO_3)_4$:Yb^{3+} laser crystal," J. Cryst. Growth **265**(1-2), 154–158 (2004).
14. L. Gudzenko, M. Kosmyna, A. Shekhovtsov, W. Paszkowicz, A. Sulich, J. Domagała, P. Popov, and S. Skrobov, "Crystal growth and glass-like thermal conductivity of $Ca_3RE_2(BO_3)_4$ (RE = Y, Gd, Nd) single crystals," Crystals **7**(3), 88 (2017).
15. P. H. Haumesser, R. Gaumé, J. M. Benitez, B. Viana, B. Ferrand, G. Aka, and D. Vivien, "Czochralski growth of six Yb-doped double borate and silicate laser materials," J. Cryst. Growth **233**(1-2), 233–242 (2001).
16. J. L. Xu, C. Tu, Y. Wang, and J. L. He, "Multi-wavelength continuous-wave laser operation of Yb: $Ca_3Gd_2(BO_3)_4$ disordered crystal," Opt. Mater. **33**(11), 1766–1769 (2011).
17. H. J. Zeng, Z. L. Lin, W. Z. Xue, G. Zhang, Z. Pan, H. Lin, P. Loiko, X. Mateos, V. Petrov, L. Wang, and W. Chen, "SESAM mode-locked Yb:$Ca_3Gd_2(BO_3)_4$ femtosecond laser," Appl. Sci. **11**(20), 9464 (2021).

132.166.160.47 {ts '2022-11-21 10:14:46'}